JOURNAL OF PROPULSION AND POWER
Vol. 35, No. 6, November–December 2019

Propellant Atomization for Porous Injectors

J. C. Deeken,* D. I. Suslov,† M. Oschwald,‡ and S. Schlechtriem§
DLR, German Aerospace Center, 74239 Hardthausen, Germany
and
O. J. Haidn¶
Technical University of Munich, 85748 Garching, Germany

DOI: 10.2514/1.B37569

Porous injectors represent an alternative injection concept to coaxial injectors for rocket engine applications using gas/liquid propellant combinations such as liquid oxygen (LOX)/hydrogen (H_2). This paper summarizes the main design features of porous injectors and proposes a mechanism of atomization for porous injectors that is considerably different to the atomization mechanism for coaxial injectors. The results of hot-fire test campaigns are presented, in which several parameters relevant to the injection process were varied: the injection velocities and momentum fluxes, the combustion chamber Mach number at the beginning of the nozzle contraction, and the LOX injector diameter. All hot-fire tests were conducted at P8 test facility for high pressure combustion research at the DLR site of Lampoldshausen with 50-mm-diameter combustion chambers operated with LOX/H_2 at sub- and supercritical chamber pressures between 30 and 100 bar. The results presented here are supporting the proposed mechanism of atomization and allow derivation of some general design guidelines for porous injectors.

Nomenclature

d	=	diameter, m
g	=	gas phase
J	=	J number, momentum flux ratio of gas to liquid
L	=	length, m
L^*	=	characteristic chamber length, m
l	=	liquid phase
Ma	=	Mach number
p	=	pressure, $kg/(m \cdot s^2)$
p'	=	axial pressure gradient, $kg/(m^2 \cdot s^2)$
t	=	throat
u	=	velocity, m/s
We	=	Weber number
x	=	axial position, m
ϵ_c	=	nozzle contraction ratio
η_{c^*}	=	combustion efficiency
κ	=	ratio of specific heat
ρ	=	density, kg/m^3
σ	=	surface tension, kg/s^2

Subscripts

CC	=	cylindrical chamber section
CoG	=	center of gravity
EoC	=	end of combustion
Inj	=	injection plane
norm	=	normalized
theo	=	theoretical
0	=	stagnation condition

Received 8 March 2019; revision received 8 July 2019; accepted for publication 9 July 2019; published online Open Access 30 August 2019.

*Group Leader, Rocket Engine Department, Institute of Space Propulsion; Jan.Deeken@dlr.de.
†Group Leader, Rocket Engine Department, Institute of Space Propulsion; Dmitry.Suslov@dlr.de.
‡Department Head, Rocket Engine Department, Institute of Space Propulsion; Michael.Oschwald@dlr.de.
§Head of Institute, Institute of Space Propulsion; Stefan.Schlechtriem@dlr.de.
¶Institute for Flight Propulsion; Haidn@lfa.mw.tum.de. Associate Fellow AIAA.

I. Introduction

SHEAR-COAXIAL injectors represent the state of the art for injectors used in gas-/liquid-fueled rocket engines, especially for the high-performance cryogenic propellant combination LOX/H_2. Injector heads with shear-coaxial elements, when designed properly, offer good atomization performance, and therefore high combustion efficiency. Their behavior has been studied extensively over the last decades. The atomization process is based on the shear forces between a dense and slow liquid jet and a surrounding low-density fast gas stream. These shear forces induce the breakup of the large-diameter inner liquid jet into small-diameter droplets, which readily evaporate. The atomization is usually characterized by dimensionless parameters such as 1) the Weber number, 2) the velocity ratio (VR), or 3) the momentum flux ratio between both propellants at the injector tip. Early investigations on shear-coaxial atomization behavior provided minimum values for these parameters to ensure stable and efficient combustion [1]. Changes in the design of shear-coaxial injectors were introduced to increase both the combustion efficiency and the margin toward the onset of combustion instabilities. For example, recessing the central tube with respect to the faceplate to a certain degree results in increased combustion stability [2].

These favorable aspects of shear-coaxial injectors come with some disadvantages. Because the atomization process is controlled by the shear forces induced by the large velocity difference between both propellants, the injector geometry has to be tightly controlled, especially with respect to the concentricity of the coaxial propellant streams. Nonconcentricity of a coaxial injector element can result in severe losses in terms of atomization quality, and therefore combustion efficiency.

Another disadvantage is the offdesign behavior of the coaxial injector. This dependency stems from the fact that every coaxial injector is designed for a certain operating point. The geometrical layout of the injector elements ensures that important dimensionless parameters of injection do not fall below certain thresholds over the desired regime of operation. The dimensions of an individual injector element define the injection velocities for certain operating conditions, which in turn define the relevant dimensionless parameters [3]:

$$We_g = \frac{\rho_g (u_g - u_l)^2 d_l}{\sigma} \tag{1}$$

$$\mathrm{VR_{gl}} = \frac{u_g}{u_l} \tag{2}$$

$$J = \frac{\rho_g u_g^2}{\rho_l u_l^2} \tag{3}$$

For gas/liquid propellant combinations, a change in chamber pressure (throttling) results in a change of the gas-phase density, whereas the liquid propellant is approximately constant in density. This change affects the aforementioned parameters through the propellant density ratio itself and the resulting variation in injection velocities. Throttling of coaxial injectors can therefore lead to reduced combustion performance.

To address these disadvantages of the coaxial injector principle, a novel injection concept for gas/liquid propellant combinations has been investigated over the last decade, both experimentally and numerically [4–11]. It aims at combining the favorable combustion performance and stability of a conventional coaxial injector with a drastically reduced manufacturing complexity. This new injection concept was named the "advanced porous injector (API)."

A similar concept was explored by Carlile and Quentmeyer [12] and also by Pavli et al. [13]. For both publications, the porous injector concept was not the main focus of investigation and little information regarding injector performance was presented. The general idea of porous injection of propellants can be traced back to Kahrs and Corbett [14]. They investigated the premixing of (hypergolic) propellants inside a porous material before injection as well as the reaction of injected oxidizer with a fuel cooling film provided by transpiration cooling through a porous chamber liner material. The authors already identified the possible benefits of porous injection, such as reduced manufacturing complexity as well as good throttling capability. However, none of the aforementioned publications provided a detailed explanation of the atomization mechanism for the various investigated injection concepts that use porous materials for the injection of one or more propellants.

This publication addresses the design and the atomization mechanism of the API porous injector concept, which is explained in more detail in Sec. II.A. It aims at systematically identifying the dominant parameters that govern the atomization process and control combustion efficiency.

II. Porous Injection

A. Typical Layout of Porous Injectors

A porous injector consists of a large number of small-diameter tubes for the injection of the high-density liquid propellant (LOX), which are distributed over a porous faceplate covering the entire chamber cross section. This porous faceplate is used to inject the low-density gaseous propellant (e.g., H_2). This approach is similar to past applications of porous media as faceplate material (e.g., RL-10 and space shuttle main engine). In these applications, a small percentage of the fuel mass flow is injected through the porous faceplate as faceplate coolant, whereas the main fuel mass flow is injected through conventional coaxial elements. In the case of the API-type porous injector, the entire fuel mass flow is injected through the porous media, and is therefore providing excellent cooling to the faceplate. A schematic drawing of such a porous injector is given in Fig. 1a. Figure 1b shows a typical arrangement of such a combination of small-diameter LOX tubes and a porous faceplate made of sintered bronze. In this case, the inner LOX post diameter was 1.5 mm. The injection area for the gaseous propellant is very large as compared to the fuel annulus of a shear-coaxial injector. The resulting injection velocity on the fuel side is very low. The injection conditions at the LOX tube tip are very different from those present for coaxial injectors. Typical injection conditions for both injector concepts for the propellant combination LOX/gaseous hydrogen (GH_2) are summarized in Table 1. Jet breakup by shear forces close to the injector tip can be considered negligible for porous injectors. On the other hand, the small diameter of the LOX injector tubes provides a smaller initial jet diameter, and therefore smaller rapidly evaporating liquid structures. The choice of a small injector diameter on the LOX side is possible because no annular gaps have to be manufactured for a porous injector. The construction of a coaxial injector with comparably small LOX injector diameters would result in extremely small annular gaps with corresponding high efforts for manufacturing and quality assurance.

Table 1 Typical injection parameters of porous (API) and coaxial injectors

		Porous injectors	Coaxial injectors
Injection velocity: LOX	m/s	10 . . . 30	20 . . . 30
Injection velocity: H_2	m/s	5 . . . 15	200 . . . 400
Momentum flux ratio J	— —	0.003 . . . 0.01	≥6.5
Weber number	— —	10^2 . . . 10^4	≥10^5

B. Atomization Mechanism of Porous Injectors

The process of propellant atomization and mixing in the case of a porous injector is vastly different from coaxial injectors. The large fuel injection area results in exceedingly low injection velocities. Considering typical parameters of injection for coaxial injectors (e.g., Weber number, velocity, and momentum flux ratio), this should result in poor atomization and mixing quality leading to poor combustion performance. However, multiple hot-fire test campaigns showed a very good combustion performance of porous injectors, which is comparable to and exceeding that of coaxial injectors [8]. Obviously, an alternative process of atomization and mixing has to be the dominant mechanism for porous injectors.

The proposed atomization process of a porous injector is based on the observation of an anchored flame at the LOX injector tip during steady-state operation. This finding was reported by Lux et al. [4]. They used an optically accessible combustion chamber with a total window length of 100 mm to investigate the near-injector region of a porous injector and found the OH^* flame emissions to start at the injector tip. Lux et al. demonstrated well-anchored flames for LOX/GH_2 at 135 K and LOX/gaseous methane (GCH_4) at 260 K.

Figure 2 illustrates the individual steps of the atomization process of a porous injector in chronological order. First, the propellants are injected in the combustion volume at their respective velocities (Fig. 2a). Because initial shear forces close to the injector tip are

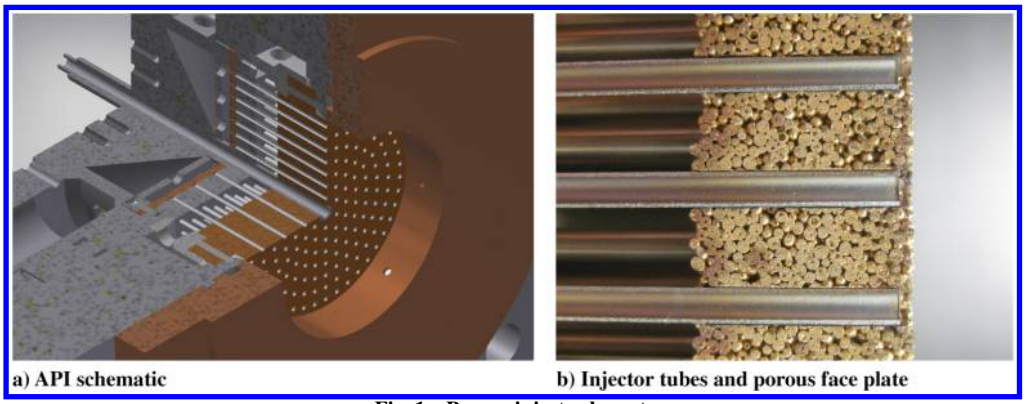

Fig. 1 Porous injector layout.

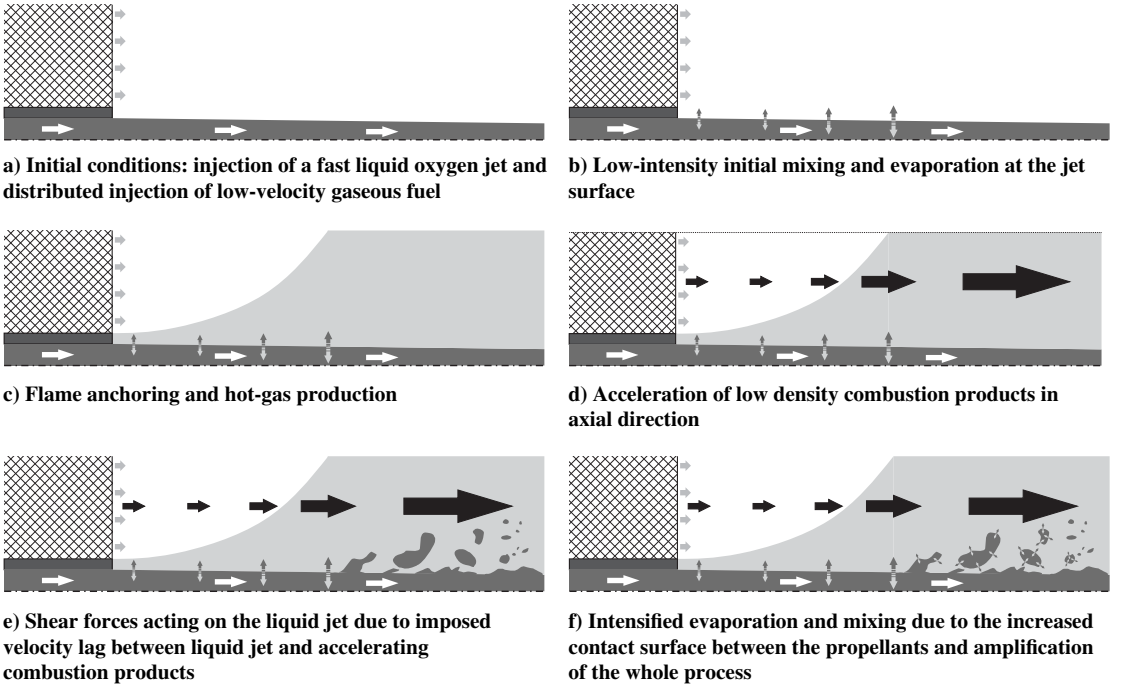

a) Initial conditions: injection of a fast liquid oxygen jet and distributed injection of low-velocity gaseous fuel

b) Low-intensity initial mixing and evaporation at the jet surface

c) Flame anchoring and hot-gas production

d) Acceleration of low density combustion products in axial direction

e) Shear forces acting on the liquid jet due to imposed velocity lag between liquid jet and accelerating combustion products

f) Intensified evaporation and mixing due to the increased contact surface between the propellants and amplification of the whole process

Fig. 2 Illustration of the successive steps of the atomization scheme of a porous injector.

negligible, little to no primary atomization takes places. However, the jet surface is disturbed, resulting in a small contact surface increase. Due to the anchoring flame, evaporation at the disturbed jet surface is enhanced and a diffusion flame is maintained. This diffusion flame produces low-density combustion gases (Figs. 2b and 2c). Continuity requires these combustion gases to accelerate in axial direction (Fig. 2d). With more and more mass added to the low-density gaseous phase in the axial direction, the hot-gas velocity increases. Because the LOX jet is initially only mildly disturbed, and because of its high inertia, the acceleration of the LOX jet is negligible in the near-injector region. The growing velocity difference between the accelerated combustion products and the slow LOX jet results in growing shear forces acting on the liquid jet. These shear forces lead to a disintegration of the liquid jet and the production of droplets and larger liquid structures (Fig. 2e). The production of smaller liquid structures increases the relevant surface area for evaporation and mixing of the propellants (Fig. 2f). The rate of hot-gas production is further increased. The whole process is self-amplified until a maximum of the velocity difference is reached. The droplet ability to follow the main flow is improved with diminishing droplet size: either due to atomization and/or evaporation. Therefore, the velocity difference decreases with decreasing size of the liquid or high-density structures. Evaporation gains the upper hand over atomization processes.

In principle, the atomization mechanism of a porous injector is based on shear forces, just like the atomization process of a coaxial injector. In contrast to the later, the shear forces are not applied on the liquid jet at the injector tip but are a result of the processes taking place in the combustion chamber. The driving forces of the atomization process are therefore not directly determined by the injection conditions at the injector faceplate. The process of atomization of a porous injector sketched previously is nonetheless influenced by certain parameters of injection. These parameters include the liquid jet injection velocity and momentum, the combustion chamber subsonic Mach number, and the liquid jet injector diameter.

The influence of the liquid jet injection velocity and momentum, which is changing the length of the reaction zone, is discussed in Sec. IV.A. The maximum combustion chamber subsonic Mach number determines the highest possible differential velocity between the hot combustion gases and the low-velocity liquid jet. This Mach number is in turn determined by the chamber contraction ratio and typically ranges between 0.2 and 0.4. This influence is discussed in Sec. IV.B. The liquid jet injector diameter determines the scale of the initial length scale of unmixedness of the propellants in the combustor. This parameter has a profound effect on droplet sizes (also for coaxial injectors). Its influence on the combustion behavior of porous injectors is discussed in Sec. IV.C.

III. Experimental Investigations

The combustion characteristics of porous injectors have been investigated in multiple hot-fire test campaigns at European research test bench P8 in Lampoldshausen [15]. Subscale combustion chambers with an inner diameter of 50 mm have been used to generate the results presented here. The investigated injector configurations covered the whole faceplate area. Due to the realistic wall heat fluxes, no optically accessible combustion chambers could be used. The results presented here are solely based on temperature and pressure measurements of the combustion process. Even without optical images, interesting features of the combustion process can be deduced from these measurements. The combustion processes for a given configuration of the injector, combustion chamber, and injection conditions were characterized by the overall combustion efficiency (Sec. III.B) and by an evaluation of the axial pressure profile in the cylindrical combustion chamber (Sec. III.C), which is an indicator for the heat release profile in the combustion chamber. The influence of the injection conditions, the chamber subsonic flow velocity, and the injector dimensions on these two quantities is reported in Sec. IV.

A. Experimental Setup

1. *Injector Heads*

The experimental findings reported here were obtained using three different API configurations, which are summarized in Table 2. All injector configurations are designed for a combustion chamber diameter of 50 mm and feature a central igniter tube with an outer diameter of 6 mm. The porous faceplate covers the entire cross section of the combustion chamber, excluding the LOX injector cross sections and the igniter tube cross section. The porous faceplate was made from sintered bronze. The three injector configurations presented here differ in size and arrangement of the LOX injector tubes.

Initial configuration API50-68 (shown in Fig. 3b) features 68 LOX injectors with an inner diameter of 1.5 mm. The LOX injectors are positioned in a checkerboard-like arrangement with a circular outer

Table 2 Geometrical parameters of the investigated API head configurations

		API50-136	API50-68	API50-36
Number of LOX injectors	— —	136	68	36
Inner/outer diameter of LOX injectors	mm	1.1/1.6	1.5/2.0	2.0/2.6
Total LOX injection area (relative to API50-68 total LOX injection area)	%	99.7	100	94.1
Total LOX injector circumference (relative to API50-68 total LOX injector circumference)	%	135.9	100	70.6
LOX post length/inner LOX diameter	— —	40.1	30	22.5

row of injectors to assure a uniform outer injector to wall distance. The influence of injection conditions and hot-gas Mach numbers on the combustion behavior was characterized with this injector configuration.

The influence of the LOX injector diameter and initial propellant contact surface were investigated using two different configurations: API50-126 (Fig. 3a) and API50-36 (Fig. 3c). They feature 126 small-diameter and 36 large-diameter LOX injectors, respectively. The total number and size of the LOX injectors of each of these injectors were chosen to provide a total LOX injection area similar to the baseline configuration: API50-68. Therefore, comparable chamber pressures and mixture ratios result in comparable injection velocities at the injector outlet for all injector configurations. Nevertheless, the initial contact surface between LOX and GH_2, represented by the sum of the LOX injector circumferences, is changing by a factor of two between API50-36 and API50-126. In both cases, the LOX injectors are arranged in a specific pattern with a 60 deg symmetry, which grows from a hexagonal shape in the center to a circular pattern in the outer injector row.

The bottom row of Fig. 3 shows the expected influence of the LOX pattern of all three injector configurations on the mixture ratio distribution. The local mixture ratio is determined by creating a virtual streamtube around each LOX injector by means of a Voronoi decomposition of the faceplate area. The injected fuel mass flow is assumed to be uniform across the entire faceplate surface, whereas the LOX mass flow is also assumed to be the same for each LOX injector. The fuel injection area accounting for a single LOX injector *i* is the fraction of the porous faceplate surface, which is located closer to injector *i* than to any other LOX injector. The LOX injector patterns used for API50-126 and API50-36 (Figs. 3d and 3f) exhibit a better mixture ratio homogeneity than the initial API50-68 pattern (Fig. 3e).

2. *Combustion Chambers*

All experiments reported here were conducted using modular subscale combustion chambers with an inner diameter of 50 mm. The combustion chambers used consist of a variable number of interchangeable water-cooled cylindrical copper segments and a final water-cooled nozzle segment. Chamber segments with specialized sensor equipment can be easily added if needed. Different chamber configurations were used, depending on the physical phenomenon to be investigated. The main geometrical features of these chamber configurations are summarized in Tables 3 and 4.

Initial investigations to cover the impact of varying injection conditions were performed with a single combustion chamber configuration. To evaluate the axial pressure evolution in the combustion zone (see Sec. III.C), this combustion chamber setup featured a specialized chamber segment of 100 mm in length equipped with nine static pressure sensors. The resulting fine axial resolution allowed for an identification of the main features of the axial pressure profile close to the injector faceplate. The rest of the cylindrical section consisted of four 50-mm-long chamber segments, with each providing an additional pressure measurement.

To address the influence of a varying maximum hot-gas velocity in the subsonic combustor part on the combustion behavior (Sec. IV.B), three different combustion chamber configurations had to be used. To reliably isolate this effect, the chamber Mach number had to be varied without changing the characteristic chamber length. The basic setup was identical to the chamber configuration used to characterize the

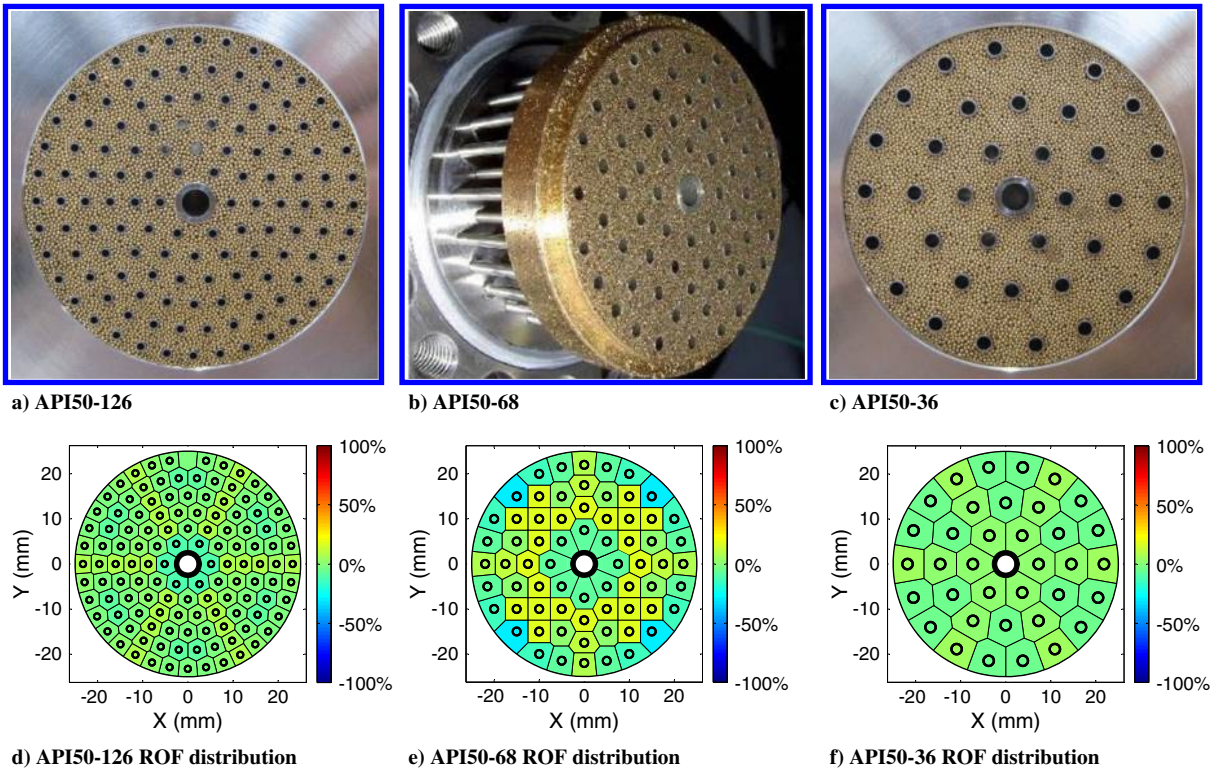

Fig. 3 Investigated injector head configurations (top row) and corresponding mixture ratio distributions (bottom row).

Table 3 Geometrical parameters of the combustion chamber configurations used

	Injection conditions (Sec. IV.A)	Hot-gas Mach number (Sec. IV.B)	Injector dimensions (Sec. IV.C)
Nozzle throat diameter d_t, mm	28	See Table 4	28
Nozzle contraction ratio ϵ_c	3.2		3.2
Cylindrical chamber length L_{CC}, mm	300		250
Characteristic chamber length L^*, mm	1044		885

Table 4 Geometrical properties of combustion chamber variations for investigation of chamber Mach number influence

	Configuration I	Configuration II/IV	Configuration III/V
Nozzle throat diameter d_t, mm	28	31.62	35.36
Nozzle contraction ratio ϵ_c	3.2	2.5	2.0
Cylindrical chamber length L_{CC}, mm	211	261	311
Characteristic chamber length L^*, mm	725.4	697.8	664.7
Chamber Mach number Ma_{CC}	0.19	0.245	0.312
Chamber velocity u_{EoC} (at 80 bar and ROF = 5), m/s	315	405	517

injection condition influence, and it featured the same 100 mm pressure sensor segment. The number of downstream 50 mm segments and the nozzle diameter were chosen to provide different contraction ratios, and therefore chamber Mach numbers, at comparable L^* values. The three configurations are shown in Fig. 4, and their main characteristics are summarized in Table 4. The second and third configurations are subdivided into two configurations each (II/IV and III/V), depending on the operational conditions during the experiments (see Sec. III.A.3).

Injector configurations API50-126 and API-36 were tested together with a different combustion chamber setup, which consisted of a single 250 mm cylindrical segment and a 28-mm-diameter nozzle segment. The instrumentation of this cylindrical segment was designed to provide a similar axial resolution in the most relevant

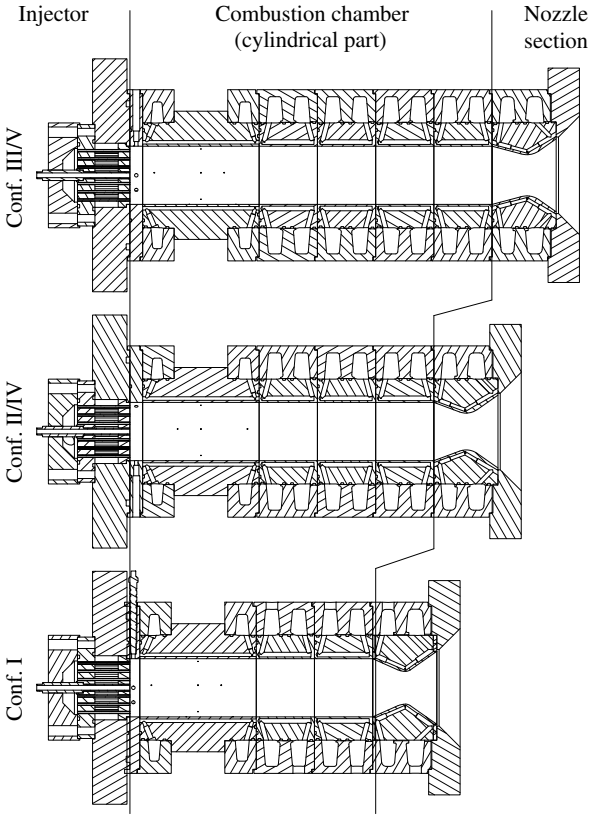

Fig. 4 Combustion chamber variations for investigation of chamber Mach number influence: configurations (Conf.) I, II/IV, and III/V (from bottom to top).

near-injector region, as in the aforementioned 100 mm pressure sensor segment.

3. Experimental Conditions

All experiments reported here used the propellant combination LOX/GH_2. Typical propellant inlet temperatures were 120 K for oxygen and 105 K for hydrogen. Depending on the test goals, different propellant mass flows, chamber pressures, and mixture ratios were set.

To assess the influence of varying injection conditions on the combustion behavior of a porous injector, injector configuration API50-68 was operated at several combustion chamber pressure levels ranging from 30 to 100 bar. This pressure range covers the sub-, trans-, and supercritical regimes with respect to liquid oxygen with a critical pressure of 50.4 bar. The mixture ratio was five in all cases. Due to the compressible nature of gaseous hydrogen, the fuel injection velocity remained approximately constant, whereas the oxidizer injection velocity was scaling with the injected oxidizer mass flow rate, and therefore with the chamber pressure. Consequently, different velocity differences of the oxidizer to fuel ($DVOF = u_{O_2} - u_{H_2}$ m/s) and momentum flux ratios of the oxidizer to fuel [$MROF = (\rho_{O_2} \cdot u_{O_2}^2)/(\rho_{H_2} \cdot u_{H_2}^2)$ J^{-1}] can be evaluated.

The influence of varying the combustion chamber subsonic flow velocity was characterized using injector configuration API50-68 and three different nozzle throats with varying cross sections. Configuration I ($\epsilon_c = 3.2$) was operated at combustion chamber pressure levels ranging from 30 to 100 bar and a constant propellant mixture ratio of oxidizer to fuel (ROF) equal to five. To assess the influence of variable contraction ratios at comparable chamber pressures, configurations II ($\epsilon_c = 2.5$) and III ($\epsilon_c = 2.0$) were operated at the same pressure levels and at the same mixture ratio as configuration I. The injected propellant mass flow rates, and consequently the injection velocities, had to increase according to the nozzle throat areas of configurations II and III. To assess the influence of variable contraction ratios at comparable injection velocities, the propellant mass flow rates of configuration IV ($\epsilon_c = 2.5$) and V ($\epsilon_c = 2.0$) were chosen as identical to those of configuration I. Therefore, similar injection velocities were obtained, whereas the chamber pressure was reduced according to the relative nozzle throat area.

To characterize the influence of varying injector dimensions with injector configurations API50-36 and -126, both injector configurations were operated at chamber pressure levels ranging from 40 to 100 bar and mixture ratios of four, five, and six. All configurations were tested with the same nozzle throat diameter. Therefore, the injected propellant mass flows were identical for both injectors. Differences in the resulting injection velocities were related to the small variation of the total LOX injection area (see Table 2).

B. Combustion Efficiency Evaluation

The evaluation of the combustion efficiency is based on the methodology defined by the Joint Army-Navy-NASA-Air Force (JANNAF) Interagency Propulsion Committee [16]. A pressure port located at the downstream end of the cylindrical section is used to determine the combustion chamber pressure for the combustion efficiency evaluation. Within the frame of this paper, no absolute combustion efficiency is given. This is due to the large combined measurement uncertainties associated with evaluating propellant mass flow rates as well as pressures. Therefore, all findings reported here are based on relative changes in combustion efficiency, which can be attributed to variations of certain parameters of injection. Multiple correction factors to the calculated combustion efficiency are considered by the JANNAF methodology. Some of them, which are relevant to the reported experiments, are discussed in the following.

The heat losses due to chamber cooling are responsible for the largest deviation in combustion efficiency determination, especially because the high surface to volume ratio of the used subscale combustors is amplifying this effect. The heat removed by water cooling amounts to about 2–5% of the total heat release within the combustor. The heat load to the chamber walls is measured by temperature measurements of the cooling water and summed up over the length of the combustor. The propellant inlet enthalpies used to calculate the theoretical combustion efficiency are corrected for this heat flux.

The second biggest correction needs to be introduced due to oxidizer impurities. The injected oxidizer mass flow is containing a certain percentage of dissolved nitrogen, which is used to pressurize the LOX in the test bench run tank. The nitrogen content is constantly monitored during the test run. The theoretically achievable combustion efficiency is corrected to account for these impurities. Depending on the test conditions, the volumetric fraction of nitrogen in the oxidizer flow ranges between 1 and 3%.

Changes in effective nozzle discharge coefficient or effective nozzle cross section are also heavily influencing the combustion efficiency determination. The effective nozzle cross section determines the combustion chamber pressure for a given propellant mass flow rate. This effective nozzle cross section is influenced by the curvature shape in the throat area, which is characterized by the ratio of the upstream nozzle curvature radius to the nozzle throat radius [17]. This ratio is equal for all nozzles of the experimental setups reported here. Therefore, the influence of the nozzle curvature is neglected in the frame of this study. The change in critical mass flow for the nozzle configurations presented here (excluding boundary layer effects) is about 0.8%. Additional changes in effective throat cross section are resulting from boundary-layer effects, which are not considered in the present study.

Another correction was introduced to compare the combustion efficiency for different nozzle throat diameters, which lead to different subsonic Mach numbers in the cylindrical combustion chamber section (see Sec. IV.B). Heat addition due to reaction at a nonnegligible Mach number leads to an irreversible acceleration in the cylindrical chamber section. For negligible injection Mach numbers (which is the case for the porous injector), the total pressure ratio between injection plane and the end of the cylindrical chamber section is

$$\frac{p_{0,\mathrm{Inj}}}{p_{0,\mathrm{EoC}}} = \frac{1 + \kappa Ma_{\mathrm{EoC}}^2}{(1 + (\kappa - 1/2)Ma_{\mathrm{EoC}}^2)^{(\kappa/\kappa-1)}} \tag{4}$$

C. Axial Pressure Profile Evaluation

The heat release due to the chemical reaction of the propellants causes an acceleration of the combustion gases, which corresponds to a decrease in static pressure in the axial direction of the chamber. The static pressure at the end of the cylindrical chamber section is determined by the hot-gas properties [$\kappa = f(\mathrm{ROF})$], the combustion efficiency, and the nozzle contraction ratio. The shape of the axial pressure profile allows for some conclusions to be drawn about the axial distribution of the heat release inside the combustor volume. A large pressure gradient indicates a strong heat addition, and therefore a region of intense mixing and reaction. A constant pressure level, on the other hand, indicates a negligible propellant conversion.

A typical axial pressure profile of a porous injector operated with a cylindrical combustion chamber is given in Fig. 5a. A large number of static pressure measurements along the chamber wall is desirable for an evaluation of the axial pressure profile. These pressure taps are concentrated in a region of the combustion chamber where the largest axial pressure gradients are expected. In the case of a porous injector, this region stretches from approximately 30 to 130 mm downstream of the faceplate. Typically, most of the pressure measurements are concentrated in this region of the most intense heat release. The pressure measurements are fit to a distorted sine function (ranging from $(1/2)\pi$ to $(3/2)\pi$), which was found to capture the typical features of the axial pressure distribution: negligible pressure change directly at the injector and the downstream chamber end, and a region of large pressure variation a few centimeters downstream of the injector.

To compare the axial pressure profiles at different operating conditions, it is convenient to transfer the gathered pressure data at various locations into a small number of scalar parameters. These scalar parameters should capture the essential features of the pressure distribution. Because designers are mostly interested in the heat release distribution of an injector concept, these parameters should be based on the axial pressure gradient rather than on the axial pressure profile itself. Two parameters are defined to characterize the axial pressure distribution: the center of gravity of the axial pressure gradient profile x_{CoG}, and the position at which pressure losses become negligible x_{EoC}. Both parameters are also illustrated in Fig. 5a.

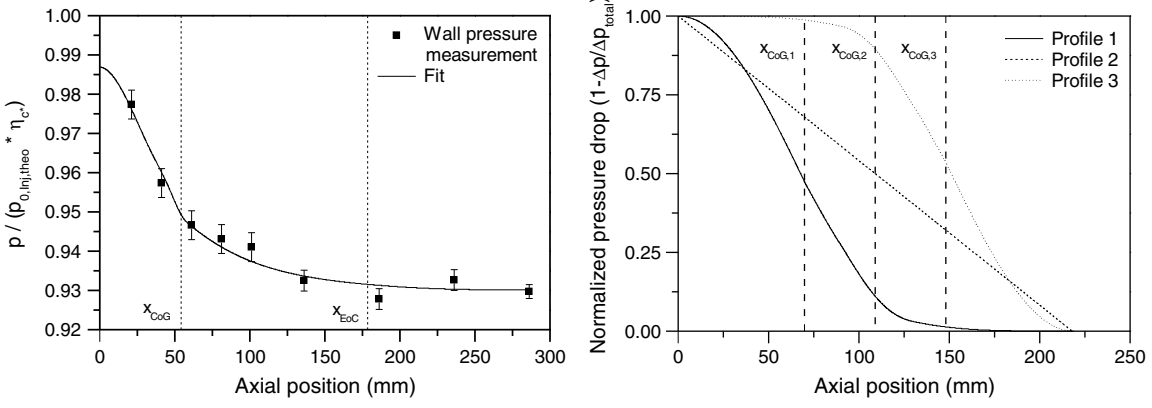

a) Typical axial pressure profile

b) Exemplary pressure distributions and corresponding values of x_{CoG}

Fig. 5 Evaluation of the axial pressure profile.

The center of gravity of the axial pressure gradient profile x_{CoG} indicates whether the pressure drop in a combustion chamber occurs close to the injector faceplate or further downstream. It is calculated as a simple center of gravity of the pressure gradient derived from static pressure measurements:

$$x_{CoG} = \frac{\int x \cdot p'(x)\,\mathrm{d}x}{\int p'(x)\,\mathrm{d}x} \tag{5}$$

Figure 5b shows some examples of arbitrary pressure profiles and their corresponding values of this parameter x_{CoG}. An early onset of a steep pressure drop results in a small value of x_{CoG}, whereas a constant negative pressure gradient results in a larger value of x_{CoG}. An efficient near-injector vaporization and mixing provide for a fast chemical reaction and heat release, and they result in a small value of x_{CoG}; whereas a large value of x_{CoG} is a clear sign for a significant delay of the aforementioned processes.

The parameter x_{EoC} on, the other hand, indicates the position at which the pressure is approaching a constant level. In a cylindrical combustion chamber, this is equivalent to a negligible rate of propellant conversion. The chamber mean flow has reached its maximum velocity in the cylindrical part of the combustion chamber, and any mixing imperfection is likely to persist beyond the nozzle throat. Such a combustion chamber could be truncated to that length without a major penalty in combustion efficiency. This position is arbitrarily defined as the position where the remaining pressure drop is smaller than 2.5% of the total pressure drop in the cylindrical chamber section.

IV. Experimental Results

A. Variation of Injection Conditions

Figure 6 illustrates the response of the porous injector to a variation in injection conditions, which are governing the atomization behavior of a classical shear-coaxial injector: specifically, the velocity and momentum flux ratio. The combustion efficiency is given as a value normalized by the maximum combustion efficiency during these test runs. No clear trend of the combustion efficiency can be detected when changing the combustion chamber pressure from sub- to supercritical conditions (Fig. 6a). Figures 6c and 6e show the same combustion efficiency values plotted against the corresponding DVOFs and MROFs, respectively. Throttling from 100 to 30 bar results in a large variation of DVOFs and MROFs. At higher pressures, the LOX injection velocity exceeds the GH_2 injection velocity. This velocity excess is inverted at lower pressures as the LOX injection velocity is linearly decreasing with chamber pressure. The momentum flux ratio of the oxidizer to fuel (equal to J^{-1}) is above unity at all conditions due to the large density ratio of LOX to GH_2. A variation of the injection conditions within these ranges does not result in any significant combustion efficiency degradation. Because the investigated ranges of the combustion chamber pressure, the velocity ratio, and the momentum flux ratio are quite large, it can be concluded that the combustion efficiency of a porous injector is controlled by different parameters.

Although no significant combustion efficiency deviations can be deduced from the test data, the axial pressure distribution in the combustion chamber shows a clear dependency on injection conditions. Figure 6b shows the values of x_{CoG} and x_{EoC} as a function of the combustion chamber pressure. The approximate extent of the main combustion zone, characterized by x_{EoC}, varies between about 170 and 180 mm. The heat release through reaction is basically finished at this axial position for all pressure levels and injection conditions investigated here. The position of the center of gravity of the axial pressure gradient x_{CoG}, on the other hand, is increased by increasing the chamber pressure and injection velocities. This correlation is also shown in Fig. 6d as a function of the injection velocity and in Fig. 6f as a function of the injection velocity ratio and momentum flux ratio. The parameter x_{CoG} is linearly increased with the increasing in LOX injection velocity, the velocity ratio of the oxidizer to fuel (VROF) and the momentum flux ratio of the oxidizer to fuel. This indicates a reaction zone that is pushed further downstream into the combustion chamber with increasing LOX injection velocity and momentum.

B. Variation of Hot-Gas Mach Number

The combustion efficiency of a porous injector is influenced by the maximum subsonic flow velocity in the cylindrical chamber section. Figure 7 shows the impact of the downstream flow velocity on the combustion efficiency and the axial pressure profile. The values shown are normalized with respect to the highest combustion efficiency attained during all tests of configurations I–V. The combustion efficiency of each configuration is varying to a limited degree (below 1%) during throttling (Fig. 7a), which is in line with the results mentioned previously (see Sec. IV.A). Figure 7c illustrates the dependency of the combustion efficiency on the maximum subsonic flow velocity u_{EoC} calculated in the cylindrical chamber section. The combustion efficiency is increasing with higher flow velocity. A higher u_{EoC} serves as an indicator for a higher-velocity difference between the hot gases and the high-inertia low-velocity LOX jets, which provides the necessary shear forces for atomization and mixing. It has to be noted that the values presented in Fig. 7c are corrected for the inevitable total pressure loss associated with higher combustion chamber Mach numbers according to Eq. (4) to directly compare the combustion efficiency at different chamber contraction ratios. Figure 7e shows the uncorrected values of $\eta_{c^*,\mathrm{norm}}$ in addition to the corrected ones. The effect of total pressure loss due to heat addition at higher Mach numbers is clearly visible. This effect is independent of injector design and purely a function of the combustion chamber contraction ratio and the resulting Mach number in the subsonic part of the combustor. Therefore, the total pressure loss and resulting combustion efficiency loss cannot be attributed to the injector. This inevitable efficiency loss at increasing subsonic Mach numbers is partially mitigated because the combustion efficiency of the porous injector is increasing with the increasing in subsonic velocity u_{EoC} (see Fig. 7c).

The influence of the chamber contraction ratio on the axial pressure evolution in the cylindrical combustion chamber section is illustrated in Fig. 7b for a supercritical operating condition at 80 bar. The relative pressure drop due to acceleration is increasing for smaller contraction ratios, as can be expected from basic theory. With a decreasing contraction ratio, and therefore an increasing subsonic chamber Mach number, the initial pressure drop indicating the main combustion zone is increasing. This can also be seen in the evaluation of x_{CoG} and x_{EoC} in Fig. 7d. The main reaction zone, represented by the value of x_{CoG}, is moving closer to the injector faceplate. The increasing possible velocity difference between the produced hot gases and the LOX jets is improving mixing, and therefore contributes to an intensified combustion. This finding, in turn, might serve as a possible explanation of the observed increase in combustion efficiency for lower contraction ratios.

C. Variation of Injector Dimensions

Apart from the influence of injection conditions and the overall chamber flowfield, the geometrical layout of the injector plays an important role for the resulting combustion process. Due to the larger number of smaller-diameter LOX posts, injector configuration API50-126 provides roughly two times the LOX jet surface area in the proximity of the LOX post as the API50-36 injector configuration. It can be expected that the proposed atomization process is enhanced by a larger production rate of hot reaction products for API50-126.

Figure 8a shows a comparison between the axial pressure profiles of both injector configurations at 60 bar and ROF = 5. The total pressure loss is not identical for both configurations. Therefore, the axial pressure was normalized to the total pressure loss of each configuration. This allows for a direct comparison of the most interesting features of the axial pressure profile. The pressure profile of API50-126 exhibits an early onset of the pressure drop associated to the main reaction zone, whereas in the case of API50-36, the onset of the pressure drop occurs further downstream and at a reduced rate. The graph also shows the associated positions of x_{CoG} and x_{EoC} for both

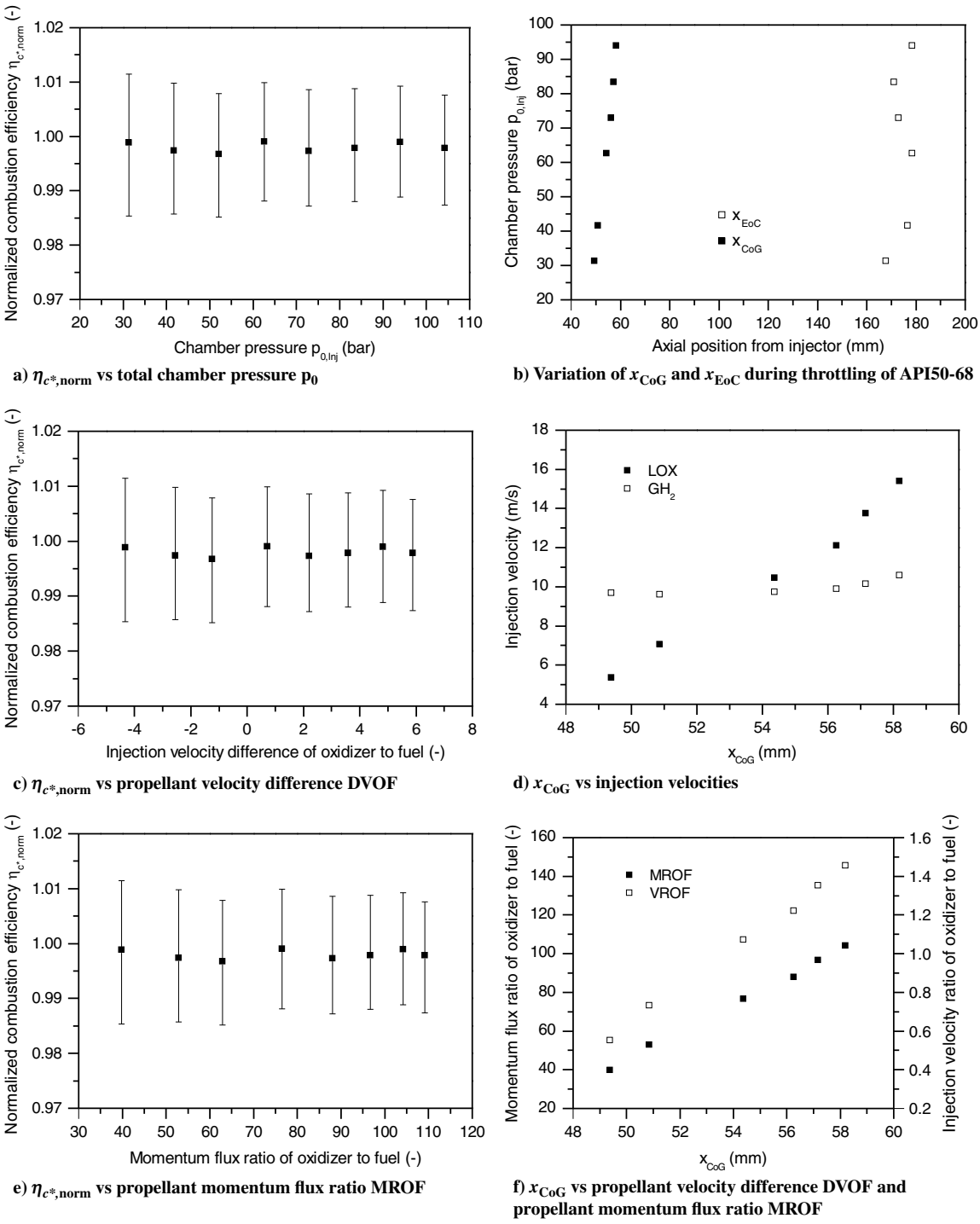

a) $\eta_{c^*,norm}$ **vs total chamber pressure** p_0

b) Variation of x_{CoG} **and** x_{EoC} **during throttling of API50-68**

c) $\eta_{c^*,norm}$ **vs propellant velocity difference DVOF**

d) x_{CoG} **vs injection velocities**

e) $\eta_{c^*,norm}$ **vs propellant momentum flux ratio MROF**

f) x_{CoG} **vs propellant velocity difference DVOF and propellant momentum flux ratio MROF**

Fig. 6 Influence of injection conditions on normalized combustion efficiency and axial pressure distribution.

injector configurations. Not surprisingly, API50-126 shows a smaller value of x_{CoG} than API50-36. The position of x_{EoC}, on the other hand, is quite similar. The total extent of the main reaction zone is therefore comparable for both injector configurations. The mean values of x_{CoG} for all operating conditions are given in Fig. 8b. The main combustion zone is always closer to the injector face for API50-126. The phenomenon of a stretched combustion zone at a higher LOX injection velocity and momentum flux ratios at higher chamber pressures is present for both injector configurations, which confirms the similar finding for API50-68 in Sec. IV.A. Interestingly, a variation in mixture ratio yields different results for both injector configurations. Although x_{CoG} is minimized at higher ROFs for API50-126, the opposite is true for API50-36. Figure 9b shows a similar tendency for the combustion efficiency as a function of the mixture ratio. Although the combustion efficiency is increasing at higher mixture ratios for API50-126, the opposite tendency can be observed for API50-36.

The correlation between x_{CoG} and the normalized combustion efficiency $\eta_{c^*,norm}$ is illustrated in Fig. 9a. For both injector configurations, a small value of x_{CoG} (and therefore an early onset of the main combustion zone) is beneficial for the overall combustion efficiency. This finding supports the presented hypothesis concerning the atomization process of a porous injector. A small value of x_{CoG} indicates a strong heat release close to the injector face, resulting in a strong acceleration of the produced hot gases. This strong acceleration provides the necessary shear forces for an improved mixing of the propellants. In Fig. 10a, the value of x_{CoG} is given as the

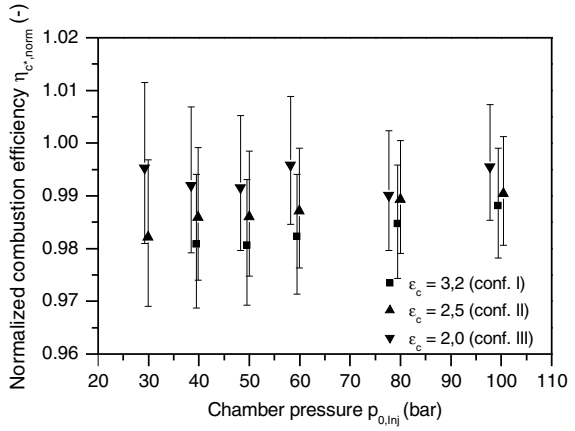

a) $\eta_{c^*,norm}$ vs total chamber pressure p_0

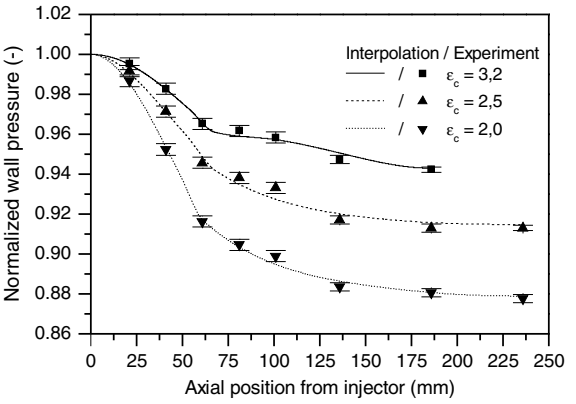

b) Axial pressure profile for three contraction ratios at 80 bar and ROF = 5

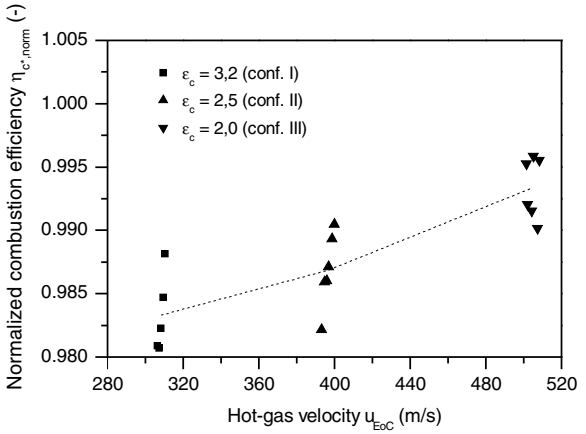

c) $\eta_{c^*,norm}$ vs subsonic flow velocity u_{EoC}

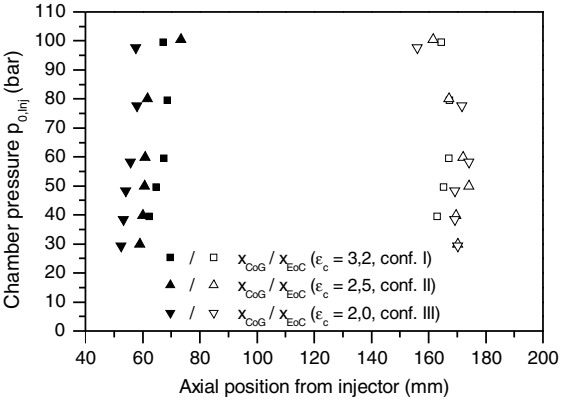

d) Variation of x_{CoG} and x_{EoC} during throttling of API50-68 with configurations I, II, and III

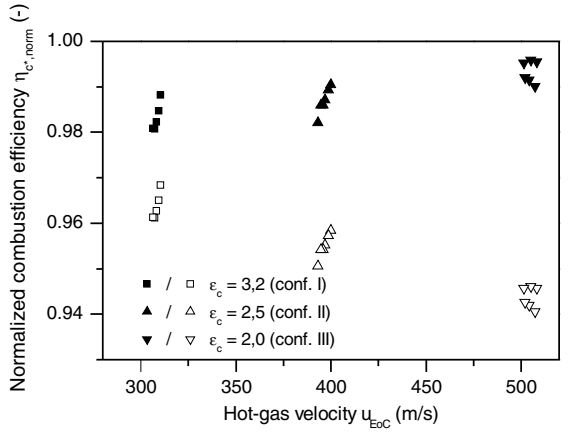

e) $\eta_{c^*,norm}$ vs subsonic flow velocity u_{EoC} with (filled symbols) and without (open symbols) correction

Fig. 7 Effect of a variation of hot-gas Mach number on normalized combustion efficiency $\eta_{c^*,norm}$ (left column) and axial pressure evolution in cylindrical combustion chamber characterized by x_{CoG} and x_{EoC} (right column).

function of a new parameter, which is the momentum flux ratio of the reacted hot-gas flow and the oxidizer at the LOX post tip (MRHGO), which is defined as follows:

$$\mathrm{MRHGO} = \frac{\rho_{\mathrm{EoC}} \cdot u_{\mathrm{EoC}}^2}{\rho_{\mathrm{O_2}} \cdot u_{\mathrm{O_2}}^2} \tag{6}$$

The parameter MRHGO correlates two momentum fluxes at different places in the combustion chamber (fully reacted flow and injected LOX) and is not achieved at any single location in the combustor. Nevertheless, this way of plotting x_{CoG} serves to better understand the influence of the mixture ratio on the general shape of the combustion zone, which is represented by the value of x_{CoG}. Higher values of MRHGO are corresponding to lower values of x_{CoG}, and therefore to the achievable combustion efficiency. As seen in Fig. 8b, a change in mixture ratio has a different effect for both injector configurations.

The small-diameter injector configuration API50-126 is showing smaller values of x_{CoG} at higher mixture ratios, although a higher mixture ratio results in a higher LOX injection momentum, which was found to have an increasing effect on x_{CoG}. Therefore, a different mechanism has to cancel this negative effect on x_{CoG}. A possible

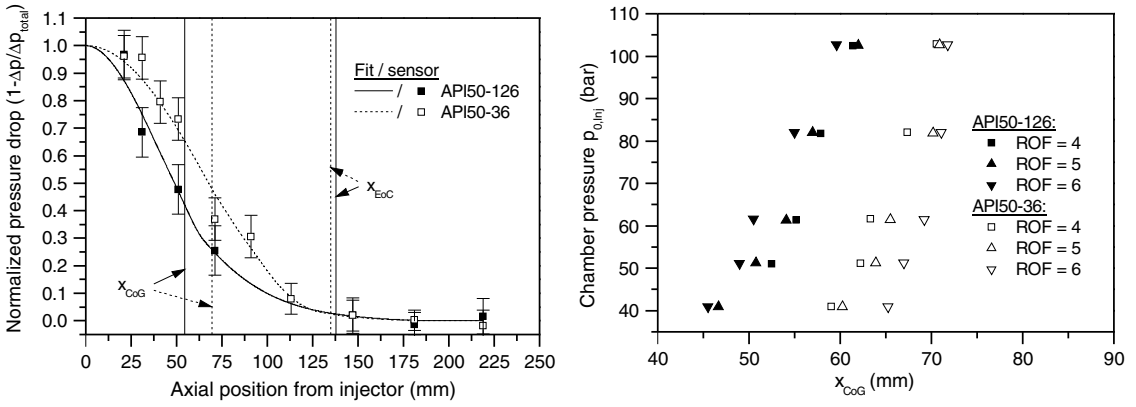

a) Axial pressure profile for two injector diameters at 60 bar and ROF = 5

b) Variation of x_{CoG} during throttling of API50-126 and API50-36 at ROF = 5

Fig. 8 Influence of the combustion chamber pressure and LOX post diameter on the axial pressure distribution.

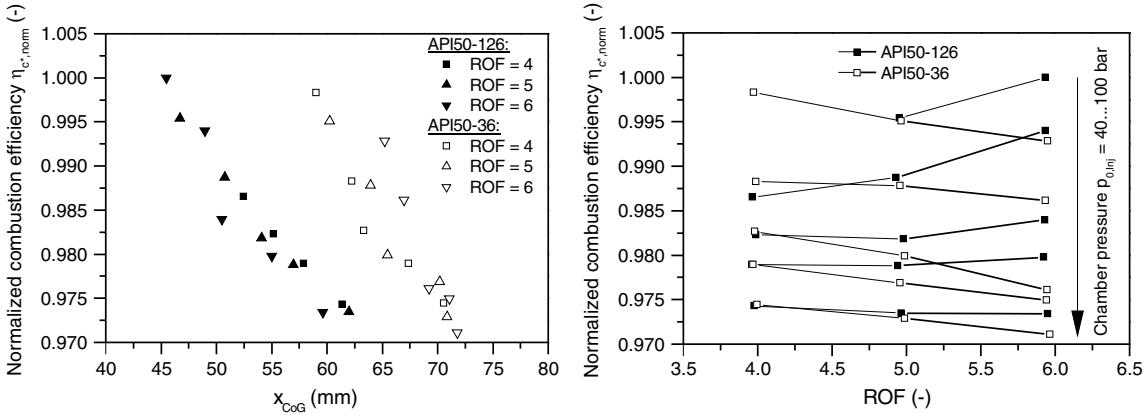

a) Relation between normalized combustion efficiencies $\eta_{c^*,norm}$ and x_{CoG} for API 126 and API 36

b) Relation between normalized combustion efficiency $\eta_{c^*,norm}$ and propellant mixture ratio for API 126 and API 36

Fig. 9 Relation between normalized combustion efficiencies $\eta_{c^*,norm}$ and x_{CoG} and ROF.

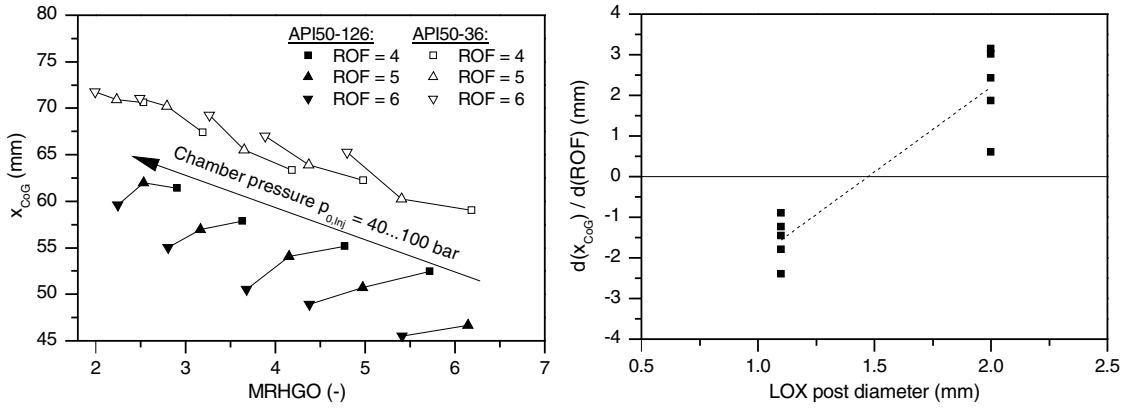

a) x_{CoG} vs momentum flux ratio of hot gas to oxidizer

b) Sensitivity of x_{CoG} toward changes in propellant mixture ratio for two different LOX post diameters

Fig. 10 Influence of momentum flux ratio of hot gas to oxidizer and LOX post diameter on x_{CoG}.

explanation is the increased energy density at mixture ratios closer to stoichiometric conditions, which is improving evaporation and an intensified production of reaction products, which is in turn further improving atomization. Because the initial propellant contact surface of API50-126 is about two times as large as for API50-36, the evaporation and diffusion process in the case of the smaller-diameter injector is benefitting more from these conditions.

On the other hand, it can be seen from Fig. 10a that the combustion behavior of large-diameter injector API50-36 is improving at lower mixture ratios. In this case, the adverse effect of high LOX injection momentum is dominating. This adverse effect can be mitigated by reducing the mixture ratio. Due to the smaller propellant contact surface, this injector configuration does not benefit as much from improved evaporation and diffusion conditions close to the injector face.

The sensitivity of x_{CoG} toward changes in mixture ratio is illustrated in Fig. 10b for both injector configurations. As mentioned previously, API50-126 is showing a decreasing value of x_{CoG} for higher mixture ratios, whereas API50-36 is exhibiting the opposite behavior. The mean of both injector configurations is connected by the dashed line. A simple linear interpolation between both

configurations would indicate a neutral behavior for the LOX post diameter of about 1.5 mm, which is the LOX post diameter for the API50-68 configuration.

V. Conclusions

The presented data from hot-fire tests of different porous injector configurations allow for an assessment of the presented hypothesis for the atomization process of a porous injector. The positive effects of increased chamber flow velocities (Sec. IV.B) and smaller injector diameters (Sec. IV.C), as well as the negative effect of liquid oxygen (LOX) injection momentum (Sec. IV.A), were clearly demonstrated. The observed sensitivity of the combustion process toward these parameters has been explained by the proposed atomization mechanism (Sec. II.B). Some general guidelines for the design of porous injectors of the "advanced porous injector (API)" type can be deduced from the results presented here.

The proposed atomization mechanism is based on the experimental observation of a stable anchored flame at the LOX post tip. This flame produces the accelerating hot-gas environment responsible for a fast and efficient atomization process. It is not known if a lifted flame could support the observed efficient combustion in a similar way.

The LOX injection velocity has a profound impact on the combustion behavior. High LOX injection velocities result in a main reaction zone enlarged in the axial direction and higher values of x_{CoG}, which was found to correlate with reduced combustion efficiency. A proper design of an API-type porous injector should therefore aim for low LOX injection velocities, which can be achieved by a high total LOX injection area or a reduced propellant mixture ratio.

The design of a porous injector has to be done in close conjunction with the combustor. At a given L^* value, the choice of the combustion chamber contraction ratio directly influences the injector performance. If weight or size constraints, or other considerations, necessitate a chamber design with a low contraction ratio, a porous injector is able to partially mitigate the inevitable total pressure loss due to heat addition in the cylindrical chamber section.

Apart from the LOX injection velocity, the physical size of the LOX injectors heavily influences the atomization process. Figure 10a implies that, for all cases investigated here, a smaller LOX post diameter is desirable in terms of the axial pressure gradient and combustion efficiency. However, there might be constraints due to manufacturing complexity or faceplate integrity, which dictate the use of larger-diameter LOX posts. It was found that smaller-diameter LOX posts (less than 1.5 mm; see Fig. 10b) perform even better at higher ratio of oxidizer to fuel (ROF), which is the case for main combustion chamber applications. Larger-diameter LOX posts (greater than 1.5 mm; see Fig. 10b), on the other hand, do not perform as well as small-diameter posts. This disadvantage can be somewhat mitigated at lower ROFs due to the reduced LOX injection momentum. This effect might be beneficial in the case of preburner applications.

Future work will be conducted to demonstrate the applicability of the proposed atomization mechanism for other liquid/gas propellant combinations, such as LOX/CH_4. With lower fuel injection temperatures, special emphasis needs to be placed on the phenomenon of a lifted flame, which is known to occur for LOX/CH_4 under certain conditions.

The API concept offers several advantages as compared to state-of-the-art coaxial injectors, namely, a low sensitivity toward changes in injection conditions, a good offdesign performance, as well as a more compact heat release zone in the combustor [8]. The last point especially makes it a very attractive choice for an injector concept for expander-based engine cycles. Due to these favorable qualities, the Liquid Upper Stage Demonstrator Engine (LUMEN) currently under development will feature an API-type porous injector.

Acknowledgments

The authors would like to thank the members of the P8 team for their contributions to the test campaigns, which yielded the experimental results presented in this paper.

References

[1] Hulka, J., and Hutt, J. J., "Instability Phenomena in Liquid Oxygen/Hydrogen Propellant Rocket Engines," *Liquid Rocket Engine Combustion Instability*, edited by V. Yang, and W. E. Anderson, Vol. 169, Progress in Aeronautics and Astronautics, AIAA, Washington, D.C., 1995, pp. 39–71, Chap. 2.

[2] Kendrick, D., Herding, G., Scouflaire, P., Rolon, C., and Candel, S., "Effects of a Recess on Cryogenic Flame Stabilization," *Combustion and Flame*, Vol. 118, No. 3, 1999, pp. 327–339. doi:10.1016/S0010-2180(98)00168-0

[3] Lasheras, J. C., and Hopfinger, E. J., "Liquid Jet Instability and Atomization in a Coaxial Gas Stream," *Annual Review of Fluid Mechanics*, Vol. 32, No. 1, 2000, pp. 275–308. doi:10.1146/annurev.fluid.32.1.275

[4] Lux, J., Suslov, D., and Haidn, O., "On Porous Liquid Propellant Rocket Engine Injectors," *Aerospace Science and Technology*, Vol. 12, No. 6, 2008, pp. 469–477. doi:10.1016/j.ast.2007.11.004

[5] Deeken, J., Suslov, D., Haidn, O., and Schlechtriem, S., "Combustion Efficiency of a Porous Injector During Throttling of a LOX/H2 Combustion Chamber," *Progress in Propulsion Physics*, Vol. 2, 2011, pp. 251–264. doi:10.1051/eucass/201102251

[6] Suslov, D., Deeken, J., and Haidn, O., "Investigation of the API-Injection Concept in a LOX/LH2 Combustion Chamber at GG/PB Operation Conditions," *48th AIAA/ASME/SAE/ASEE Joint Propulsion Conference & Exhibit*, AIAA Paper 2012-3857, 2012. doi:10.2514/6.2012-3857

[7] Deeken, J., Suslov, D., Schlechtriem, S., and Haidn, O., "Impact of Injection Distribution on Cryogenic Rocket Engine Stability," *Progress in Propulsion Physics*, Vol. 4, 2013, pp. 149–166. doi:10.1051/eucass/201304149

[8] Deeken, J., Suslov, D., Rackemann, N., and Preuss, A., "Combustion Performance and Stability of a Porous Injector Compared with a State-of-the-Art Coaxial Injector," *Space Propulsion 2014*, SP-2969154, Cologne, 2014.

[9] Zhukov, V., and Haidn, O., "Analytical Study of Stationary Temperature Field in Transpiration Cooled Porous Wall," *Journal of Aerospace Engineering*, Vol. 227, May 2012, pp. 873–881. doi:10.1177/0954410012446899

[10] Zhukov, V., and Suslov, D., "Measurements and Modelling of Wall Heat Fluxes in Rocket Combustion Chamber with Porous Injector Head," *Aerospace Science and Technology*, Vol. 48, Jan. 2016, pp. 67–74. doi:10.1016/j.ast.2015.10.021

[11] Zhukov, V. P., and Heinrich, K. P., "Evaluation of the Grid Convergence for a Rocket Combustion Chamber with a Porous Injector," *Acta Astronautica*, Vol. 158, May 2019, pp. 438–443. doi:10.1016/j.actaastro.2018.08.002

[12] Carlile, J. A., and Quentmeyer, R. J., "An Experimental Investigation of High-Aspect-Ratio Cooling Passages," NASA TM-105679, 1992. doi:10.2514/6.1992-3154

[13] Pavli, A. J., Kacynski, K. J., and Smith, T. A., "Experimental Thrust Performance of a High-Area-Ratio Rocket Nozzle," NASA TP-2720, 1987.

[14] Kahrs, J., and Corbett, A., "Propellant Injection Through Porous Media," *AIAA 3rd Propulsion Joint Specialist Conference*, AIAA Paper 1967-0463, 1967. doi:10.2514/6.1967-463

[15] Koschel, W., and Haidn, O., "P8—The New French/German Test Facility for High Pressure Rocket Engine Combustion Research," *International Journal of Hydrogen Energy*, Vol. 23, No. 8, 1998, pp. 683–694. doi:10.1016/S0360-3199(97)00088-8

[16] Powell, W. B., "Simplified Procedures for Correlation of Experimentally Measured and Predicted Thrust Chamber Performance," NASA TM-33-548, 1973.

[17] Kliegel, J. R., and Levine, J. N., "Transonic Flow in Small Throat Radius of Curvature Nozzles," *AIAA Journal*, Vol. 7, No. 7, 1969, pp. 1375–1378. doi:10.2514/3.5355

J. C. Oefelein
Associate Editor